Available online at www.sciencedirect.com
SCIENCE DIRECT®
ELSEVIER
International Journal of Solids and Structures 42 (2005) 6356–6375
INTERNATIONAL JOURNAL OF SOLIDS and STRUCTURES
www.elsevier.com/locate/ijsolstr

Structural changes in granular materials: The case of irregular polygonal particles

C. Nouguier-Lehon *, E. Vincens, B. Cambou

LTDS, Ecole Centrale de Lyon, UMR CNRS 5513, 36 Av Guy de Collongue, 69134 Ecully Cedex, France

Received 9 July 2004; received in revised form 7 April 2005
Available online 7 July 2005

Abstract

This paper presents a series of numerical simulations of biaxial tests performed on assemblies of two-dimensional irregular polygonal particles. Each sample is prepared with a technique similar to dry pluviation. Different aspect ratios (1–3) are considered and the behavior of granular samples is analyzed from both a global and a local point of view. More precisely, the influence of the particle aspect ratio on both inherent (initial) and induced anisotropy is investigated. New internal variables which are related to the orientation of particles are proposed. They give new insight into the specific mechanisms that control the behavior of irregular polygonal materials. Associated to global variables, they demonstrate the existence of a *critical state* irrespective of the investigated aspect ratios. However, for materials with higher aspect ratios (2 and 3), their inherent anisotropy prevents any extensive reorganization, this means that, within the range of usual strains considered in civil engineering, the particle reorientation remains in progress and considerable deformations are required to reach the critical state.

Keywords: Granular material; Polygonal particle; Aspect ratio; Biaxial test; Anisotropy; Internal state; Critical state

1. Introduction

The constitutive modelling of granular materials remains an open issue because it has proved difficult to define relevant macroscopical variables that capture the evolution of the internal state accurately. This difficulty is essentially related to the discontinuous nature of such materials and to the great changes that may affect their internal structure. Another difficulty arises as experimental tests cannot generally provide suf-

* Corresponding author. Tel.: +33 4 7218 6213; fax: +33 4 7218 6537.
E-mail address: cecile.nouguier@ec-lyon.fr (C. Nouguier-Lehon).

0020-7683/$ - see front matter © 2005 Elsevier Ltd. All rights reserved.
doi:10.1016/j.ijsolstr.2005.04.021

ficient information about the internal state of samples. This deficiency generates a bias that may prevent a good understanding and modelling of phenomena. Discrete numerical simulations of granular materials seem of great interest in this respect, as they provide information at the grain scale level throughout the loading process. They will eventually give clues to define clear internal variables for modelling.

Many analyzes dedicated to the study of two-dimensional granular materials by means of a discrete element method (DEM) have been published in the literature, but most of them have been performed on simulated samples with materials composed of either cylindrical particles (Cundall and Strack, 1979; Thornton and Barnes, 1986; Dedecker et al., 2000; Radjaï et al., 2004; Cambou et al., 2004), isotropic-shaped polygons (Mirghasemi et al., 2002; Nouguier-Lehon et al., 2003) or elliptical particles (Rothenburg and Bathurst, 1992; Rothenburg and Kruyt, 2004). Isotropic shapes give rise to specific internal states and a global material behavior which is not generally in good agreement with natural materials like sands, gravels or rocks (low peak friction angle value, low dilatancy rates,...). This bias is introduced by perfect roundness (that characterizes how smooth or sharp the edges of the particles are) and cylindricity (extrapolation of sphericity in two-dimensional context). Nevertheless, some studies have thrown valuable insight onto the mechanisms of the creation of induced anisotropy (Rothenburg and Bathurst, 1989). On the other hand, elliptical particles are only representative of a class of actual granular materials. However, they have proved to be a more realistic way to idealize the description of granular material. For example, Rothenburg and Bathurst (1992) simulated biaxial tests performed on elliptical shaped particles from an isotropic state. They investigated the influence of particle aspect ratio on the initial state (density, coordination number) and the way induced anisotropy was generated. Qualitative and quantitative relationships were obtained but specific behavior of particles with a higher aspect ratio remained difficult to explain. Moreover, when the phenomena involved in the shear bands of real sands are investigated (Oda and Kazama, 1998), it seems that rotational stiffness at contacts play a major role in strength development in granular materials. This aspect cannot be reflected using elliptical smooth particles. Consequently, in DEM, the use of particles that can develop edge-to-edge contacts seems to be a more appropriate way to model the behavior of a large amount of actual angular soils.

This paper analyzes materials composed of two-dimensional irregular polygonal particles having different aspect ratios, which corresponds to a realistic representation of a large class of real materials considered in civil engineering. Biaxial tests are simulated for different samples generated by dry pluviation of grains within a box. Each sample contains particles whose shapes belong to a group of aspect ratios (1, 1.5, 2 or 3). We investigate the role of inherent anisotropy for each sample by considering different loading directions with respect to bedding. The behavior of granular materials is presented from both a local and a global point of view. Internal variables are introduced to trace the evolution of anisotropy, and considerations with respect to the critical state are derived.

2. Conditions for the numerical simulations

2.1. Numerical context

In this paper, we present some results from two-dimensional distinct element numerical simulations performed with a program based on the *Contact Dynamics* method (Jean, 1995, 1999; Moreau, 1994, 1999). This method, initiated by Cundall and Strack (1979) for granular modelling, consists in computing the evolution of large systems of bodies using time discretization. The constituents of the granular medium are assumed to be rigid grains interacting with each other by contact, with friction or not. At each time step, the position and the velocity of each grain is computed by solving the dynamics equation, taking into account the contact forces between particles and the boundary conditions. Two principal features are peculiar to the *Contact Dynamics* method: firstly, the non-interpenetrability constraints and the Coulomb dry friction law

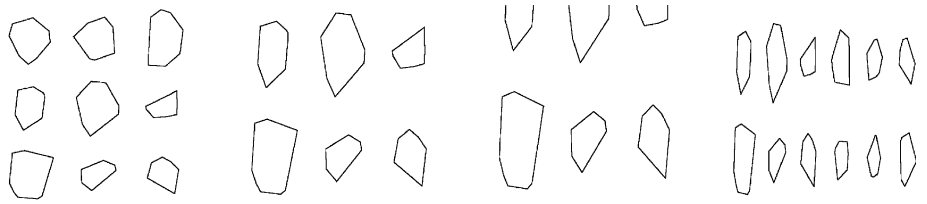

Fig. 1. Examples of grain shapes for each aspect ratio.

are treated without pseudo-elastic repulsions; secondly, in case of collisions between grains, both normal and tangential restitution coefficients are introduced within the local laws.

2.2. Definition of the shape library

In this two-dimensional numerical study, the granular media is composed of rigid convex polygonal grains with at least five vertices and at most eight vertices. Hundreds of grains with different shapes are gathered within a common *shape library*. In order to compare the behavior of granular materials in relation to the grain aspect ratio, we generated several libraries of shapes. The first one contains 500 grains with statistically isotropic shapes whose dimensions range between $d_{\min} = 0.2$ cm and $d_{\max} = 0.52$ cm following a truncated Gaussian distribution. The other libraries are deduced from this one by dilating the grains in one direction (generating the so-called aspect ratio R_a). In this analysis, four aspect ratios R_a are considered: 1, 1.5, 2 and 3. Examples of grain shapes contained in each library are shown in Fig. 1.

2.3. Preparation of numerical samples

The samples are created by pluviating the grains one by one into a rectangular box under the gravity, the grain being randomly chosen from one of the four previously defined shape libraries. Thus, four samples are generated from four different libraries. Granular materials with an aspect ratio ranging between 1 and 1.5 are classified within the family of poorly elongated materials. Most sands studied in the literature (Leighton Buzzard sand, Toyoura sand, Ottawa sand or Hostun sand among others) belong to this family. Grain aspect ratios greater than 2 are representative of elongated materials in which family we can find pebbles, but also road gravels or road surface gravels. However, most real materials are probably a mix of grains presenting different ranges of aspect ratios. The main parameters of each considered sample can be found in Table 1.

Table 1
Main characteristics of samples

Material	A	B	C	D
Aspect ratio, R_a	1	1.5	2	3
Number of grains	4789	1832	1427	1937
$d_{\max}/d_{\min}$	2.6	2.6	2.6	2.6
Local friction ratio	0.3	0.3	0.3	0.3
Normal restitution coefficient	0.2	0.2	0.2	0.2
Tangential restitution coefficient	0.1	0.1	0.1	0.1

3. Initial structure

When the grains are pluviated into a box under gravity, the granular material is organized in such a way which is specific to each shape of grain. The arrangement of the packing is investigated through the knowledge of phenomena at contacts by means of the number of coordination of grains which is the average number of contacts required for equilibrium but also by means of orientation of particles and orientation of normals at contacts.

3.1. Coordination number

In order to characterize the average number of contacts for a particle, the *coordination number* N_c is used. Table 2 shows that after deposit under gravity, the resulting N_c value depends on the aspect ratio of particles: an increased aspect ratio leads to an increased value of both N_c and e. It is clear that particle shape plays an important role in the relation between N_c and e, because the results shown in Table 2 are in complete disagreement with the usual empirical formulations (Field, 1963; Chang and Misra, 1990) which do not take particle shape into account.

3.2. Contact fabric tensor

Usually, the *contact fabric tensor* $\boldsymbol{H}$ defined by $\boldsymbol{H} = \langle \boldsymbol{n} \otimes \boldsymbol{n} \rangle$, where $\boldsymbol{n}$ is the contact normal unit vector, is used to characterize the fabric anisotropy within a granular assembly (Satake, 1978). This tensor gives some global information about the normal orientations at contact.

Experiments on two-dimensional analogical materials composed of cylindrical rods (Biarez and Wiendieck, 1963; Calvetti et al., 1997) have shown that deposit under gravity induces an initial anisotropic texture. In this study, the distribution of contact orientations for the sample with grains having an aspect ratio equal to 1 presents the two usual preferential directions around $\pm 60°$ (Fig. 2), which is similar to that encountered for media composed of circular particles. This value is linked to the most probable equilibrium

Table 2
Coordination number and void ratio values at the end of the pluviation process

Material	A	B	C	D
Void ratio	0.213	0.227	0.245	0.287
Coordination number	3.67	3.7	3.9	3.91

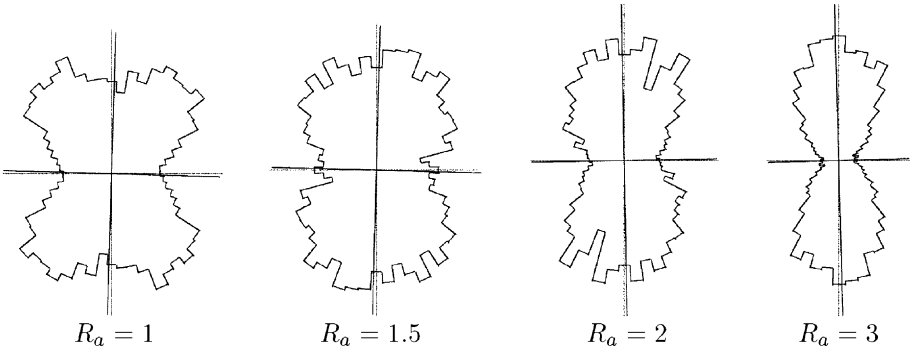

Fig. 2. Distribution of contact orientations at the end of the dry pluviation process.

position for a circular particle lying on two other particles with the same diameter. For granular materials with aspect ratios equal to 1.5, 2 or 3, the particular grain shape leads to a characteristic organization: the majority of grains lays in a position close to horizontal and the distribution of contact orientations presents a single vertical preferential direction (Fig. 2).

To study structural anisotropy changes in relation to grain shapes, a simple but relevant quantity that is able to capture the evolution of the local fabric must be defined. A scalar measurement of anisotropy b_H is proposed hereafter and is defined by the following ratio:

$$b_H = \frac{2(H_{11} - H_{22})}{(H_{11} + H_{22})}, \tag{1}$$

where H_{11} and H_{22} are the components of tensor $\boldsymbol{H}$ in directions (1) and (2), respectively the major and minor principal loading directions (Fig. 4). One can note that the definition of b_H is not strictly the ratio between the second and the first invariant of $\boldsymbol{H}$. However, this parameter will provide valuable information on the internal state of samples in relation to the principal loading directions. The values obtained for b_H clearly indicate that inherent anisotropy due to the way the samples were created is more pronounced when the aspect ratio is greater (Table 3).

3.3. Tensor of orientations

Since most grains used in these simulations present a preferential geometrical direction, anisotropy changes can also be analyzed from the point of view of particle orientation within the sample. We introduce the local tensor $\boldsymbol{a}^p$, defined for a particle p from the vectors $\boldsymbol{s}^k$ connecting the grain center of gravity G to each vertex k of the polygon by

$$\boldsymbol{a}^p = \frac{1}{2\pi} \sum_{k=1}^{N_V} \alpha^k \boldsymbol{s}^k \otimes \boldsymbol{s}^k, \tag{2}$$

where N_V denotes the number of vertices of the considered polygon and α^k is the angle between the bisecting lines of three successive vertices, as defined in Fig. 3. The major principal direction of $\boldsymbol{a}^p$ gives the current orientation of particle p. This major principal direction can only be defined for a non-isotropic tensor, so only for grains with an aspect ratio greater than 1. The polar representation of the initial orientations

Table 3
Initial microscopical characteristics of anisotropy

Material	A	B	C	D
b_H	0.15	0.26	0.47	0.8
b_A	–	0.18	0.54	0.96
S	–	1.2	1.74	2.87
$S_{\max}$	–	1.58^2	2.07^2	3.07^2

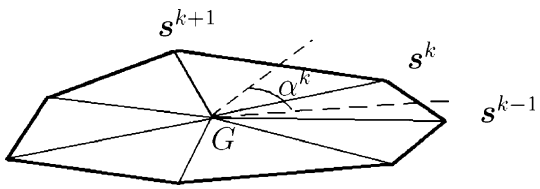

Fig. 3. Definition of angle α^k.

converges with the previous result in that, after the deposit under gravity, most grains lie within horizontal planes (Figs. 22–27). In order to characterize the maximum anisotropy of a given sample, we define parameter $S_{\max}$ by

$$S_{\max} = \frac{\langle a_{\mathrm{I}}^p \rangle}{\langle a_{\mathrm{II}}^p \rangle}, \tag{3}$$

where $\langle a_{\mathrm{I}}^p \rangle$ and $\langle a_{\mathrm{II}}^p \rangle$ are, respectively, the average of the major and minor eigenvalues of $\boldsymbol{a}^p$ over the whole sample. $S_{\max}$ is related to the aspect ratio by the relationship $S_{\max} \simeq R_{\mathrm{a}}^2$ (Table 3).

Then, to analyze the global orientation of grains, the average $\boldsymbol{A}$ of $\boldsymbol{a}^p$ over the whole sample is considered:

$$\boldsymbol{A} = \langle a^p \rangle. \tag{4}$$

From this tensor, parameter b_A can be defined in the same way as for $\boldsymbol{H}$. Another way to study the global structural changes consists in following the evolution of parameter S defined by

$$S = \frac{A_{\mathrm{I}}}{A_{\mathrm{II}}}, \tag{5}$$

A_{I} and A_{II} being, respectively, the major and minor principal values of $\boldsymbol{A}$. b_A and S both quantify the intensity of the anisotropy linked to the particle orientation (Table 3), but S gives further details: if $S = 1$, the material is not structured at all (all orientations of particles have the same occurrence probability); conversely, if $S = S_{\max}$, all particles are oriented in the same direction. Consequently, S values should evolve between 1, which corresponds to $b_A = 0$, and $S_{\max}$.

To summarize, as the aspect ratio of particles increases, the initial structural anisotropy, computed either with b_H, b_A or S, increases. The associated coordination number evolves in the same way, though the computed density tends to decrease.

4. Macroscopical analysis of simulations

Biaxial tests are simulated using the previously mentioned granular materials. For each specimen of peculiar particle shape, two simulations are performed. We call α the angle between the direction of loading and the direction of deposit (direction of gravity). First, the specimen is loaded in the direction of deposit ($\alpha = 0$). Secondly, a simulation is undertaken in a direction perpendicular to the deposit direction ($\alpha = \pi/2$). This case is illustrated by Fig. 4 together with the conditions of simulation. During simulated biaxial tests, one of the boundaries is subjected to a constant stress ($\sigma_2 = 10$ kPa) and one of the orthogonal walls is subjected to a constant velocity V until a given strain is reached. As shown in this figure, direction (1) always corresponds to the major principal direction of applied stress (associated to σ_1) and direction (2) to the minor principal direction of stress (associated to σ_2). Finally, it must be pointed out that the walls have a friction ratio equal to 0.

For particles with the largest aspect ratio, that is to say 3, a further simulation with a loading direction at $\pi/4$ is performed. Once the pluviation of the grains within a box under gravity is completed, a smaller sample is built considering walls orientated at 45° with respect to gravity (Fig. 5(a)). Particles located outside the new walls are eliminated and the new sample is rotated so that during the simulation of biaxial tests, the sample will be loaded in a direction $\alpha = \pi/4$ with respect to the bedding (Fig. 5(b)).

The results of the biaxial test simulations are represented by two diagrams. The first one emphasizes the evolution of stress ratio q/p ($q = \sigma_1 - \sigma_2$ and $p = (\sigma_1 + \sigma_2)/2$) with deformation ε_1 in direction (1). The second one illustrates the evolution of void ratio e with deformation ε_1. Finally, we must specify that

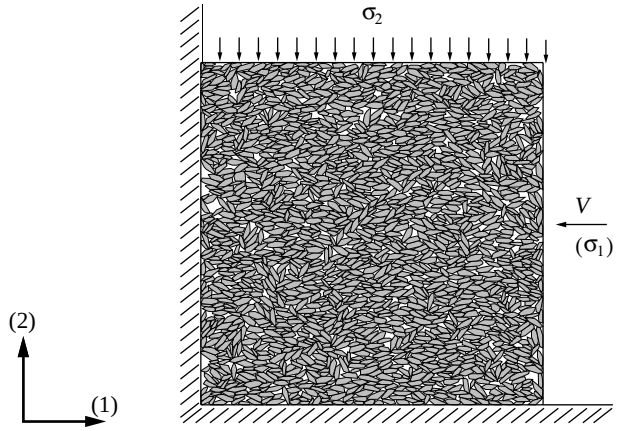

Fig. 4. Initial state for a sample ($R_a = 3$) and boundary conditions for biaxial simulations ($\alpha = \pi/2$).

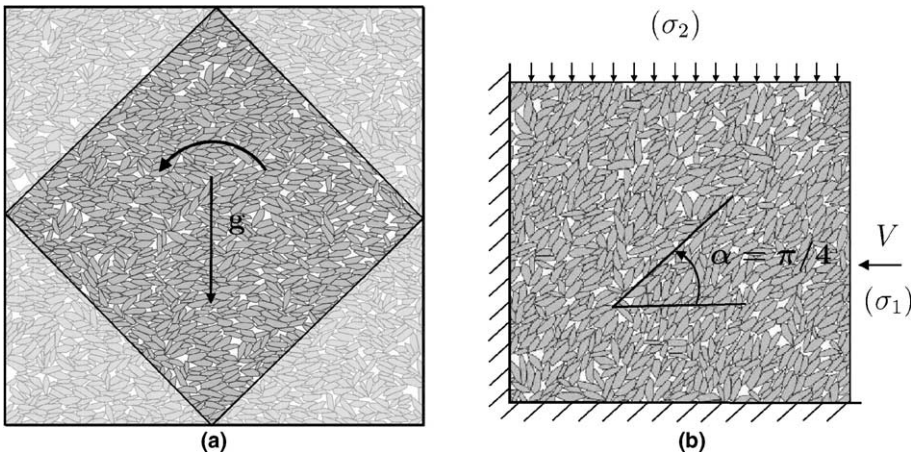

Fig. 5. Creation of a sample with a bedding angle equal to $\alpha = \pi/4$ with respect to loading (g is the direction of gravity during the initial deposit).

deformation ε_1 is defined using a large strain definition $\varepsilon_1 = \ln(h/h_0)$, h_0 and h being, respectively, the initial and the current length of the box in direction (1).

4.1. Simulations with particles having a small aspect ratio

These simulations correspond to materials whose aspect ratio is inferior or equal to 1.5. Figs. 6 and 7 illustrate the behavior of the specimens involved. For loading in the direction of deposit ($\alpha = 0$), the same trends are observed for both materials: the stress ratio quickly evolves towards a steady-state value. This high resistance that appears for strains ε_1 lower than 2% is associated with almost no contractive behavior. For the loading condition $\alpha = \pi/2$, the stress ratios increase towards a single mobilized angle at large strains ($\varepsilon_1 \geqslant 15\%$). These steady state angles are equal to 25° and 27° for materials with an aspect ratio equal to 1 and 1.5, respectively. Moreover, simulations performed on dense packing composed of such grains shows that the same steady state is reached (Nouguier-Lehon et al., 2003).

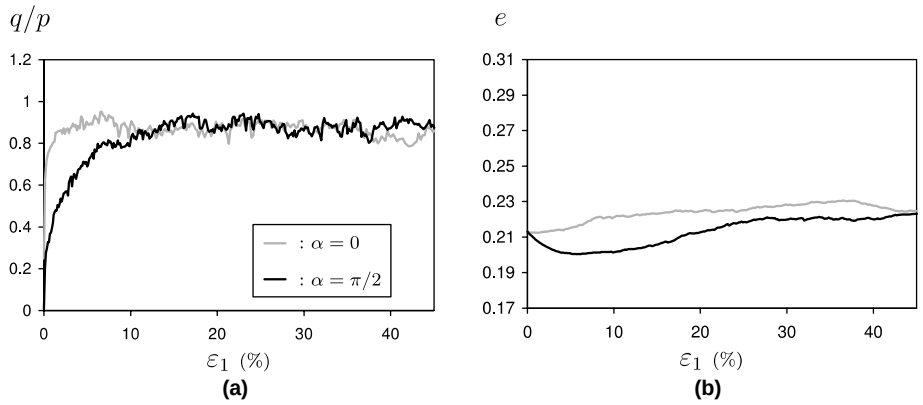

Fig. 6. Deviatoric (a) and volumetric (b) graphs for samples with $R_a = 1$.

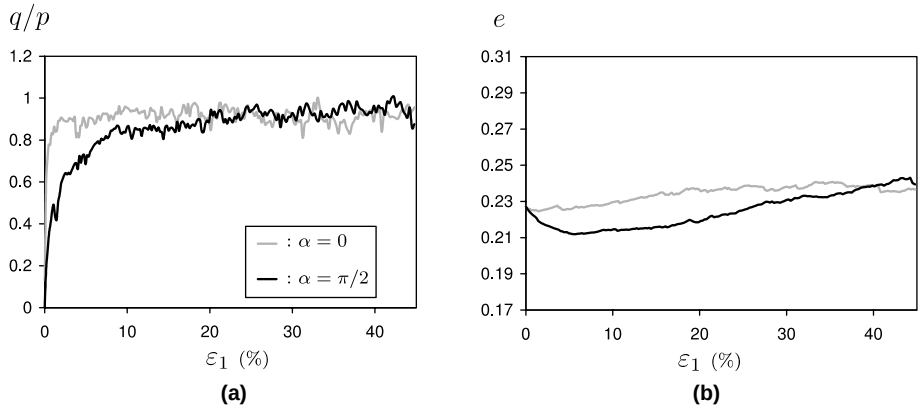

Fig. 7. Deviatoric (a) and volumetric (b) graphs for samples with $R_a = 1.5$.

The evolution of the void ratio for this class of material supports the existence of a steady state void ratio independent of loading conditions and initial density properties (Nouguier-Lehon et al., 2003) (Figs. 6(b) and 7(b)).

To conclude, the simulations performed for specimens generated with poorly elongated particles (aspect ratio up to 1.5) clearly demonstrate the existence of a critical state as defined by Roscoe et al. (1958) or Poulos (1981). In the stress space, the steady state is rapidly reached, whereas large deformations are required for the void ratio to reach this single state. Finally, a larger aspect ratio R_a seems to delay the obtention of such a reference state.

4.2. Simulations with highly elongated particles

These specimens are related to polygons with an aspect ratio equal to or greater than 2. For polygons with an aspect ratio equal to 2 (Fig. 8(a)), the stress ratio increases to a constant value irrespective of loading direction ($\alpha = 0$ or $\alpha = \pi/2$). Nevertheless, at large strains ($\varepsilon_1 = 40\%$), the void ratio of specimens has not reached a steady state yet (Fig. 8(b)) and at this stage, it is not clear whether such a state can be obtained. The analysis of the evolution of anisotropy and results obtained for the material with an elongation

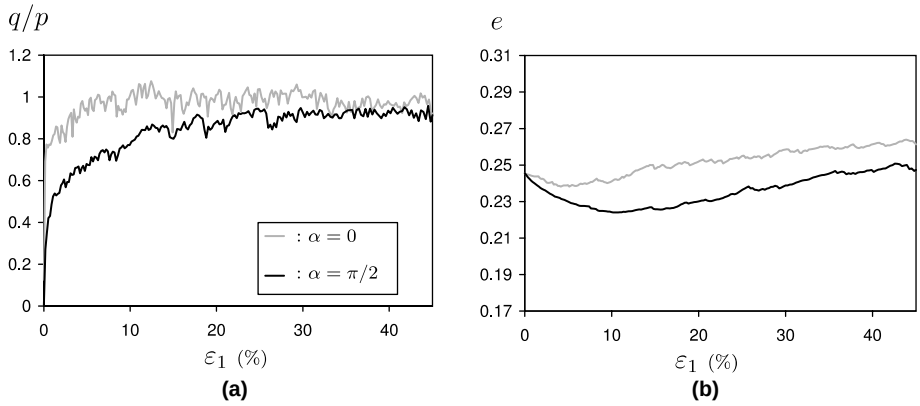

Fig. 8. Deviatoric (a) and volumetric (b) graphs for samples with $R_a = 2$.

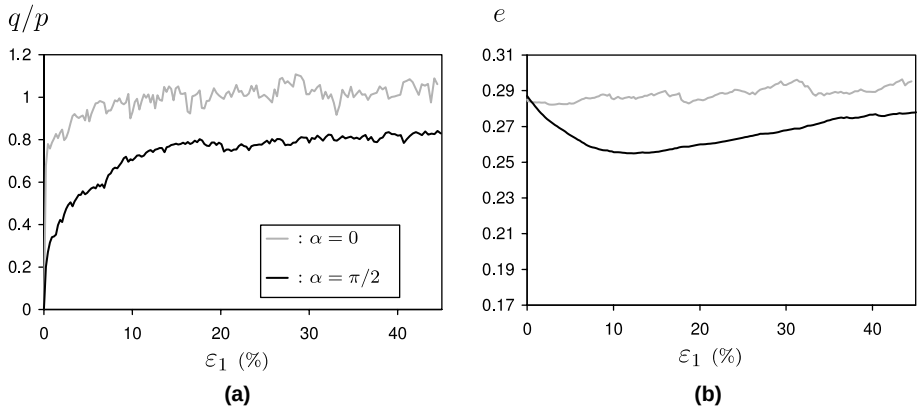

Fig. 9. Deviatoric (a) and volumetric (b) graphs for samples with $R_a = 3$.

ratio equal to 3, for which the loadings have been pursued up to a strain of 100%, will give further information in this respect.

For polygons with an aspect ratio equal to 3, a common stress state may not be reachable for different directions of loading (Fig. 9(a)). Moreover, kinematic processes within the samples does not seem to have stabilized at the considered strain $\varepsilon_1 = 40\%$ (Fig. 9(b)). Further simulation with another loading direction with respect to inherent anisotropy ($\alpha = \pi/4$) was performed and all the tests were pursued up to a strain $\varepsilon_1 = 100\%$ (Fig. 10). One can note that all the samples evolve towards a common state (stress ratio, void ratio) irrespective of loading directions, but an unusually high deformation level is required. This range of deformation (50–100%) is not considered in the case of homogeneous strains, but may easily be reached in zones of localized strains. The existence of a critical state is therefore confirmed even for materials with high aspect ratios but requires huge deformations. Another confirmation of the existence of such a reference state is given by Nouguier-Lehon et al. (2003) who found that, given a direction of loading with respect to the initial fabric, specimens with different initial densities (loose or dense) evolve towards a single state at large strains, even if the aspect ratio of particles is high ($R_a = 3$). This phenomenon is observed both in the stress ratio and the void ratio.

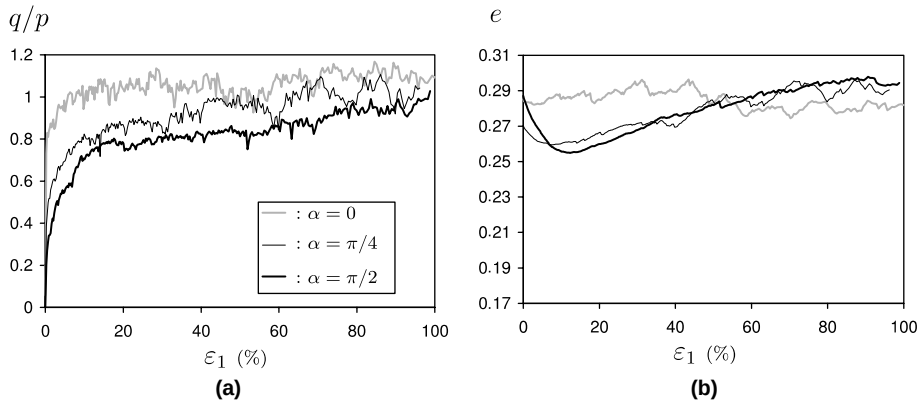

Fig. 10. Deviatoric (a) and volumetric (b) graphs for samples with $R_a = 3$.

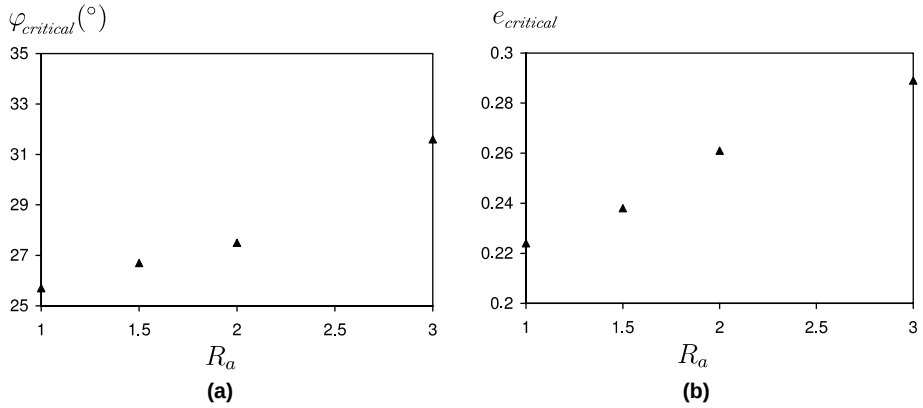

Fig. 11. Correlation between the macroscopical properties at the critical state and the aspect ratio of particles.

To conclude this part, the simulations performed on different samples generated with irregular polygons (characterized by different aspect ratios) validate the existence of the critical state as defined by Roscoe et al. (1958) or Poulos (1981), whatever the shape of involved particles. However, for loadings applied in a direction different to inherent anisotropy ($\alpha \neq 0$), this peculiar state can only be observed for very large strains (greater than 100%). A clear trend can be highlighted: the mobilized angle and the void ratio at critical state increase almost linearly with the aspect ratio of involved particles (Fig. 11(a) and (b)). Finally, one can note that the initial void ratio for the largest aspect ratio due to the pluviation of grains under gravity is very close to the critical void ratio (Table 4).

Table 4
Mechanical characteristics for each material

Material	A	B	C	D
e_{initial}	0.213	0.227	0.245	0.287
e_{critical}	0.224	0.238	0.261	0.289
$\varphi_{\text{critical}}$	25.7°	26.7°	27.4°	31.6°

5. Evolution of the local structure

Different local variables can be used to define the internal state of a granular material; four of them have been used in this study:

- the coordination number N_c (average number of contacts for a particle) which is a scalar generally linked to the compactness of the material;
- the tensor of contact orientations $\boldsymbol{H}$ which gives a measurement of the state of anisotropy;
- the tensor of particle orientations $\boldsymbol{A}$ which has been defined previously, and gives another measurement of anisotropy;
- the mean rotation of particles $\widetilde{\omega}$.

Scalar $\widetilde{\omega}$, tensors $\boldsymbol{H}$ and $\boldsymbol{A}$ are obviously linked. Different representations of these two tensors will be used in this paper: polar representations, representations in the axial system of loading (1,2) by scalars b_H for tensor $\boldsymbol{H}$, b_A and S for tensor $\boldsymbol{A}$.

5.1. Coordination number

Experimental or numerical analyzes have shown that the coordination number N_c is directly correlated to the density of the granular material, and various empirical formulations have been developed relating this number and the void ratio (Field, 1963; Chang and Misra, 1990). These formulations can only be considered as crude approximations because they do not take into account either the granulometry or the shape of particles. More precisely, while the relationship between the coordination number and the void ratio seems to be clear for particles with a high aspect ratio (Fig. 13), this is no longer true for particles with a low aspect ratio (Fig. 12). Moreover, both figures confirm that the shape of particles has a great influence on this relationship but also that the relationship "coordination number versus void ratio" highly depends on the initial internal state. This seems particularly true for particles with the greatest aspect ratio values (i.e., 2 and 3).

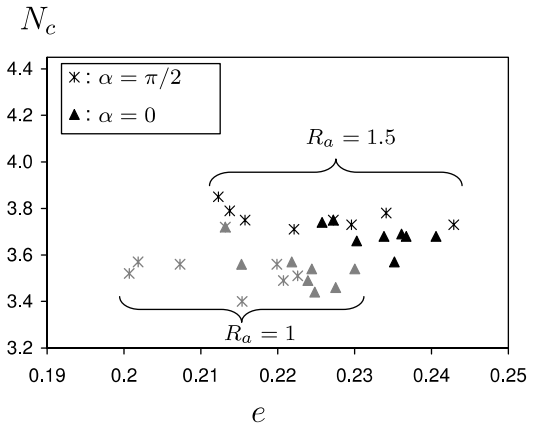

Fig. 12. Relation between the coordination number and the void ratio (aspect ratios 1 and 1.5).

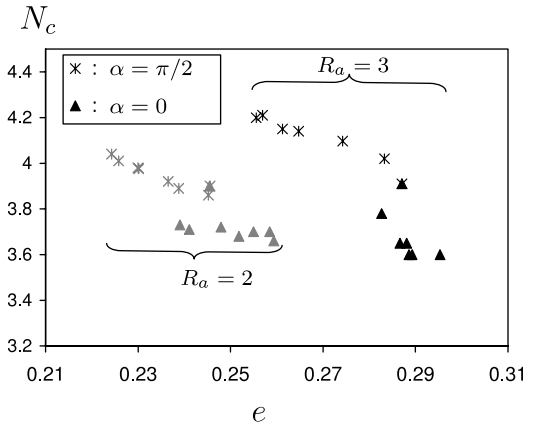

Fig. 13. Relation between the coordination number and the void ratio (aspect ratios 2 and 3).

5.2. Tensor of contact orientation

As mentioned before, the samples analyzed in this study were obtained by deposit under gravity generating the initial structured media (Section 3). Figs. 14–17 show that for the test condition $\alpha = 0$, the very deposit process has generated the major part of the overall anisotropy. Indeed, b_H slightly increases from the initial value revealing that the initial structure does not evolve very much. Actually, the evolution of the structure completely stops when ε_1 reaches 20%. By contrast, for the loadings applied in a direction different from that of inherent anisotropy ($\alpha = \pi/2$), the evolution of the deviatoric part of the fabric tensor is significant.

For the samples created with either isotropic particles (Fig. 14), or particles with a low aspect ratio ($R_a = 1.5$), a common state at large strains is reached whatever α value. More precisely, this common state

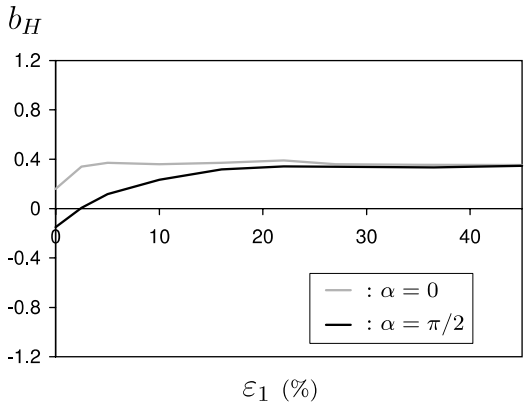

Fig. 14. Evolution of b_H for samples with $R_a = 1$.

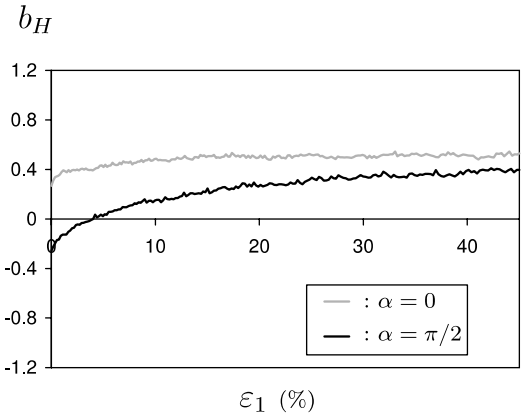

Fig. 15. Evolution of b_H for samples with $R_a = 1.5$.

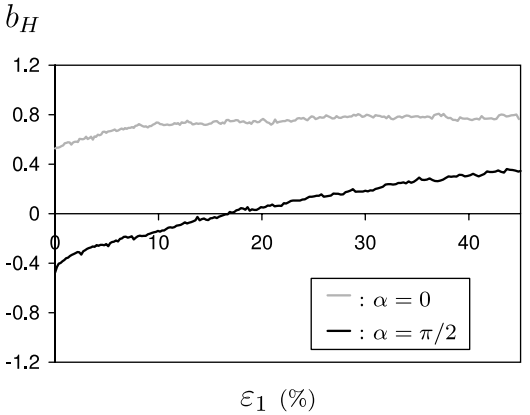

Fig. 16. Evolution of b_H for samples with $R_a = 2$.

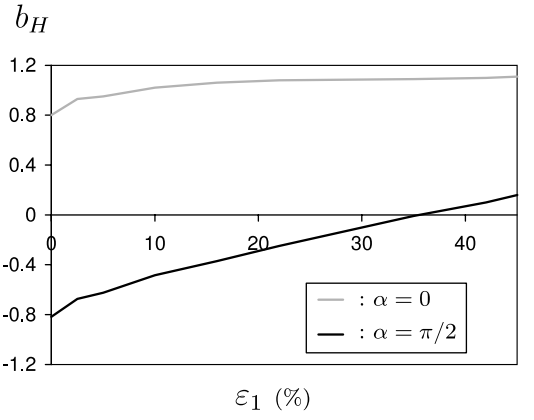

Fig. 17. Evolution of b_H for samples with $R_a = 3$.

is almost reached at the end of the simulation ($\varepsilon = 45\%$) and for $\alpha = \pi/2$, b_H is likely to increase towards the b_H value obtained for $\alpha = 0$ (Fig. 15). One can note that contact orientation within the samples is still

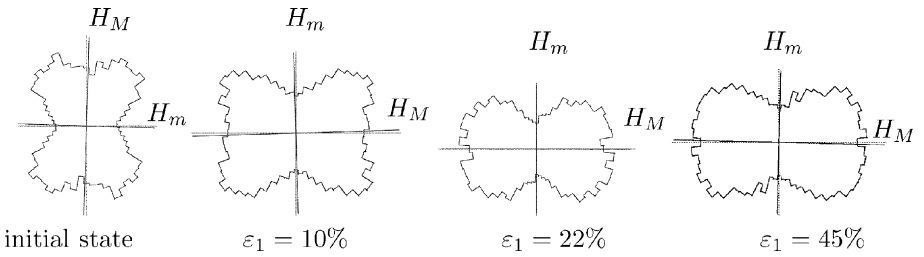

Fig. 18. Distribution of contact orientation ($R_a = 1$, $\alpha = \pi/2$).

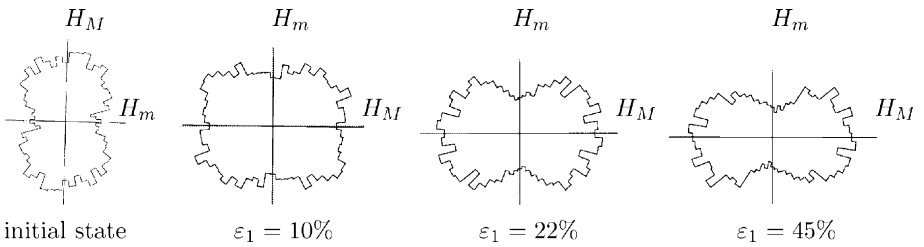

Fig. 19. Distribution of contact orientation ($R_a = 1.5$, $\alpha = \pi/2$).

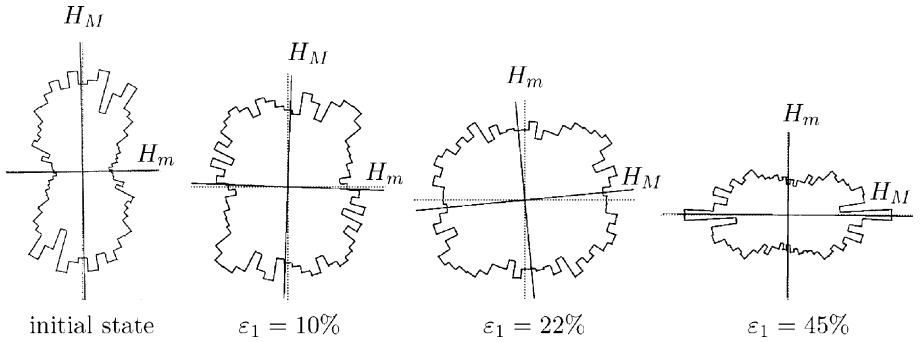

Fig. 20. Distribution of contact orientation ($R_a = 2$, $\alpha = \pi/2$).

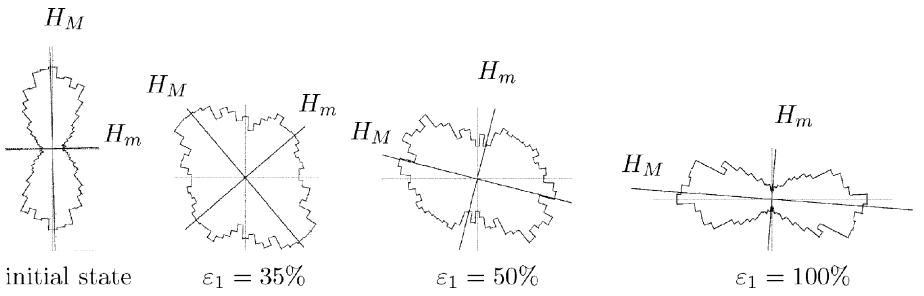

Fig. 21. Distribution of contact orientation ($R_a = 3$, $\alpha = \pi/2$).

going on for the simulation performed with a material having high elongation ratio (Figs. 16 and 17). Nevertheless, further simulations performed with the most elongated particles ($R_a = 3$) show that a common internal state is obtained when major principal strain increases up to 100% (Fig. 34) irrespective of loading direction. This means that the concept of *critical anisotropy* is relevant, but we can note that great deformations are required for the process of reorientation to be completely achieved.

The distribution of contact orientation is just presented for the loading condition $\alpha = \pi/2$, since for $\alpha = 0$ the principal directions obviously do not change. For the loading condition $\alpha = \pi/2$, different observations can be drawn in relation to the aspect ratio of particles. For particles with an aspect ratio smaller than 3 (Figs. 18–20), the principal directions of $\boldsymbol{H}$ do not change throughout the simulation, but only the major and minor principal axes change roles. Indeed, the orientations of contacts between particles change so that they tend to coincide with the direction of loading. One can note that this re-definition of principal axes is finished at small strains for isotropic granular materials and is delayed as the particles' aspect ratio R_a increases. On the contrary, for particles with an aspect ratio equal to 3 (Fig. 21), the principal directions of $\boldsymbol{H}$ show a continuous rotation as deformation ε_1 increases. This phenomenon is related to the global rotation of particles occurring in this case which will be discussed further on.

5.3. Tensor of particle orientation $\boldsymbol{A}$

This tensor only gives valuable information for particles with an anisotropic shape, consequently only the samples with an aspect ratio between 1.5 and 3 will be studied. Tensor $\boldsymbol{A}$ can be analyzed using a polar representation or using the scalar parameters b_A or S, defined in Section 3.3.

The dry pluviation method used in this work to create the samples induces a peculiar orientation of particles whose major principal axis tends to be oriented perpendicularly to gravity (Figs. 23–27). Within a polar representation, the low state of anisotropy (from tensor $\boldsymbol{A}$) is conveyed by an ellipse which almost turns into a lemniscate of Bernoulli for high states of anisotropy. The former type of graph is a

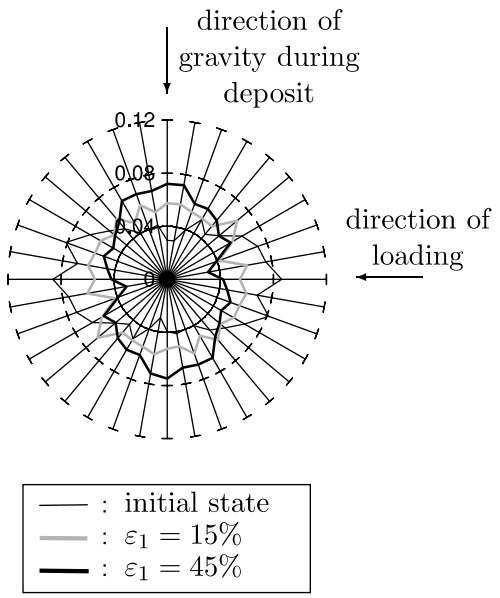

Fig. 22. Distribution of particle orientation ($R_a = 1.5$, $\alpha = \pi/2$).

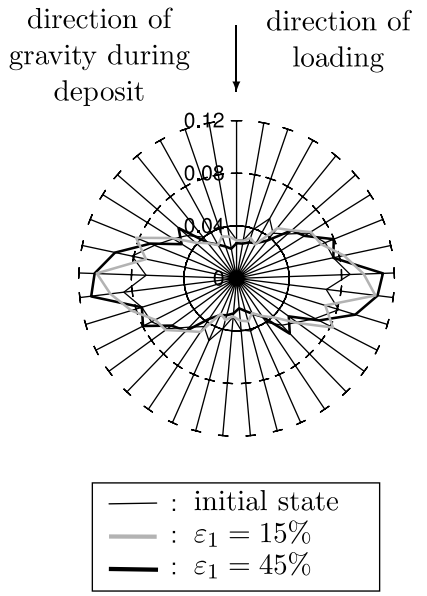

Fig. 23. Distribution of particle orientation ($R_a = 1.5$, $\alpha = 0$).

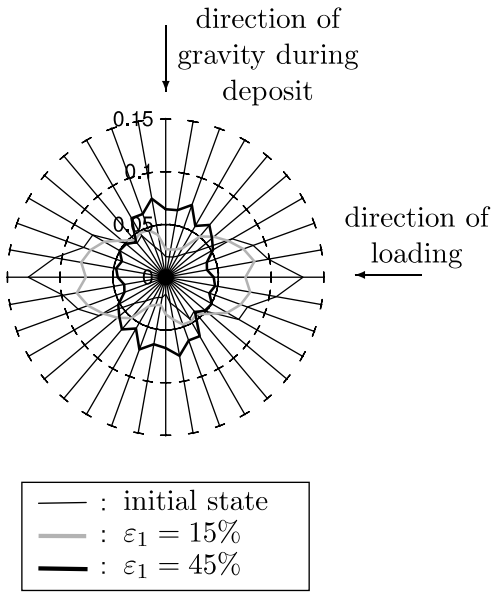

Fig. 24. Distribution of particle orientation ($R_a = 2$, $\alpha = \pi/2$).

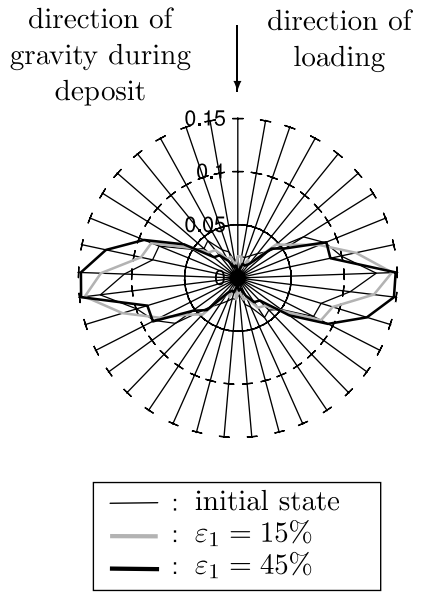

Fig. 25. Distribution of particle orientation ($R_a = 2$, $\alpha = 0$).

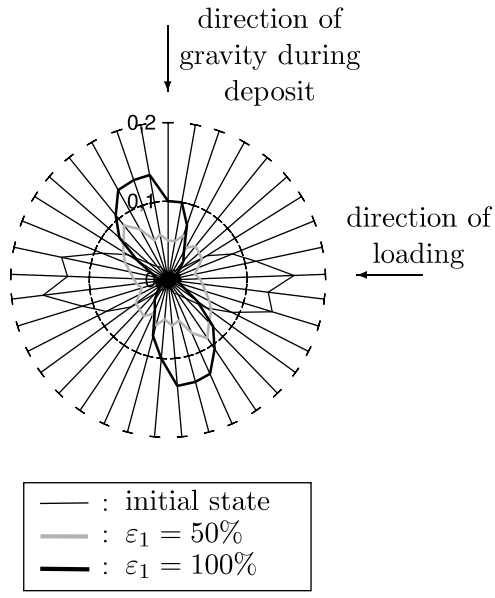

Fig. 26. Distribution of particle orientation ($R_a = 3$, $\alpha = \pi/2$).

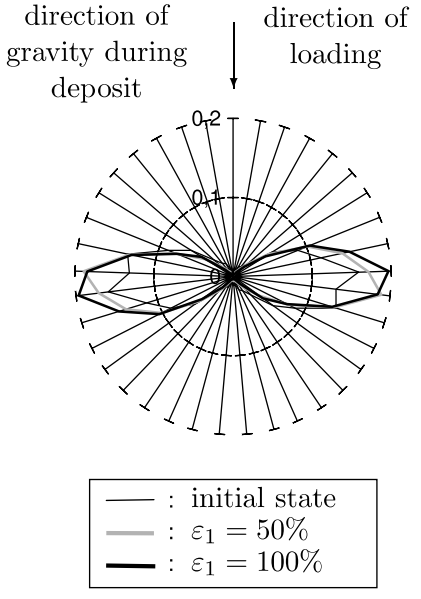

Fig. 27. Distribution of particle orientation ($R_a = 3$, $\alpha = 0$).

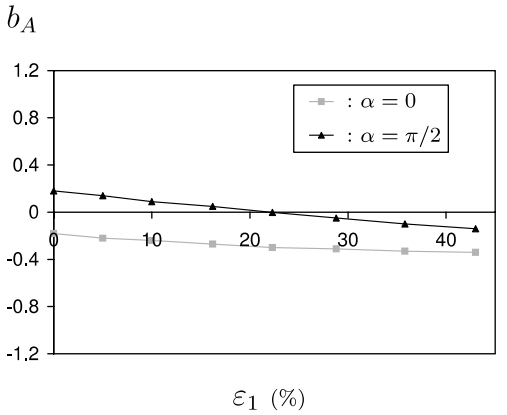

Fig. 28. Evolution of parameter b_A for samples with $R_a = 1.5$.

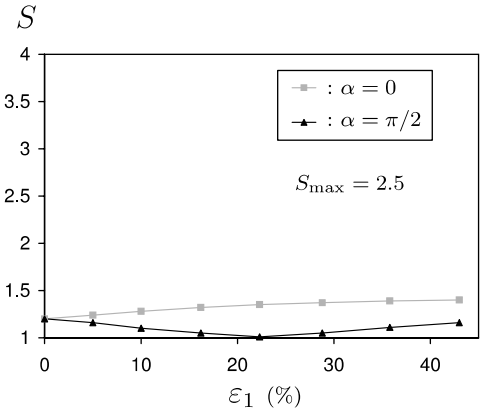

Fig. 29. Evolution of parameter S for samples with $R_a = 1.5$.

characteristic of particles with a low aspect ratio while the latter type characterizes the orientation of particles with a high aspect ratio.

When loading in the direction of gravity ($\alpha = 0$), the aspect of the graphs retains the same features, as the majority of particles are already almost all aligned in the appropriate direction.

For the loading condition $\alpha = \pi/2$, $\boldsymbol{A}$'s principal axes do not change during simulations for particles with an aspect ratio equal to 1.5 and 2 (Figs. 22 and 24). For particles with an aspect ratio equal to 3, we observe a progressive rotation of the $\boldsymbol{A}$ axes (Fig. 26). The reason for such a difference in the process of re-orientation of particles will be exposed in a further section.

As expected, when loading with $\alpha = 0$, b_A does not change signs and keeps increasing slowly in absolute value (Figs. 28, 30 and 32) indicating that the anisotropy evolves but only gently.

On the contrary, when loading in a direction perpendicular to gravity ($\alpha = \pi/2$), the b_A value greatly changes. In this case, for particles with aspect ratios equal to 1.5 and 2, the initial fabric is destroyed so that the distribution of particle orientation approaches that of a randomly distributed medium. Then, parameter S decreases to 1 which corresponds to an approximately isotropic polar representation of $\boldsymbol{A}$.

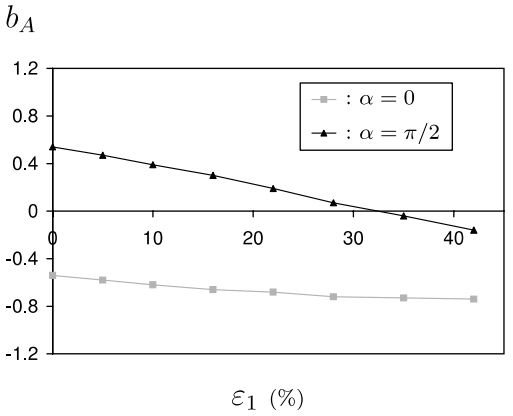

Fig. 30. Evolution of parameter b_A for samples with $R_a = 2$.

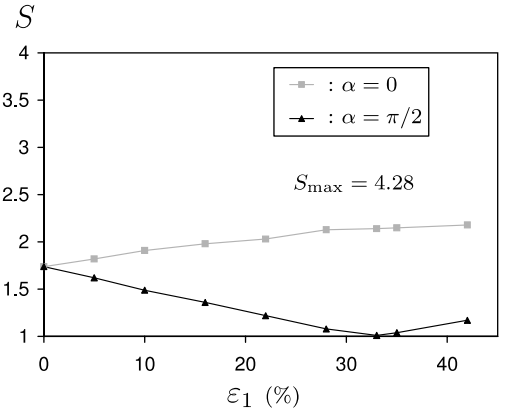

Fig. 31. Evolution of parameter S for samples with $R_a = 2$.

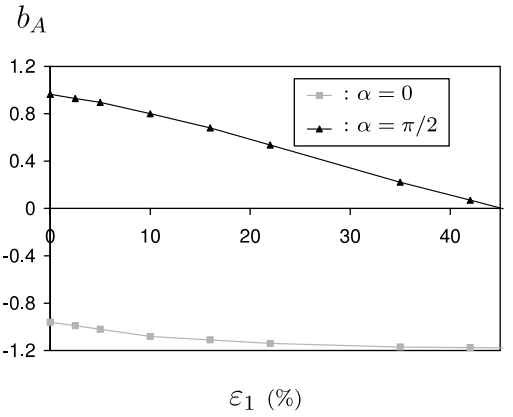

Fig. 32. Evolution of parameter b_A for samples with $R_a = 3$.

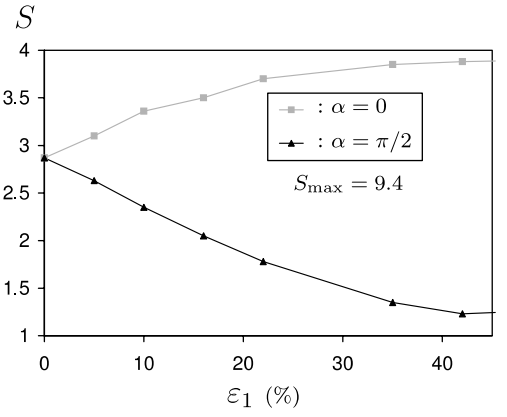

Fig. 33. Evolution of parameter S for samples with $R_a = 3$.

As loading is pursued, a new structure is progressively generated (S increases). For particles with an aspect ratio equal to 3, the completely random geometrical state is never reached during the simulation: S does not reach 1 and increases after $\varepsilon_1 = 45\%$ (also derived from Fig. 26). As a consequence, this discrete media remains oriented throughout the simulation (Figs. 29, 31, 33).

Generally, at the end of the simulations (major principal strain equal to 45%), the values obtained for b_A or S are significantly different for the two kinds of loading ($\alpha = \pi/2$, $\alpha = 0$) but, at this stage, both these variables are still evolving (especially for the loading condition ($\alpha = \pi/2$). When simulations are performed to even higher levels of strain ($\varepsilon_1 = 60\%$ for the samples with $R_a = 2$ or greater than $\varepsilon_1 = 100\%$ for the samples with $R_a = 3$), common b_A or S values are reached irrespective of loading direction ($\alpha = 0$, $\alpha = \pi/4$, $\alpha = \pi/2$) (Fig. 35). This feature validates the concept of critical state, in particular the existence of a critical anisotropy. This is consistent with the results obtained through the analysis of tensor $\boldsymbol{H}$. Nevertheless, here again, extremely large strains are required.

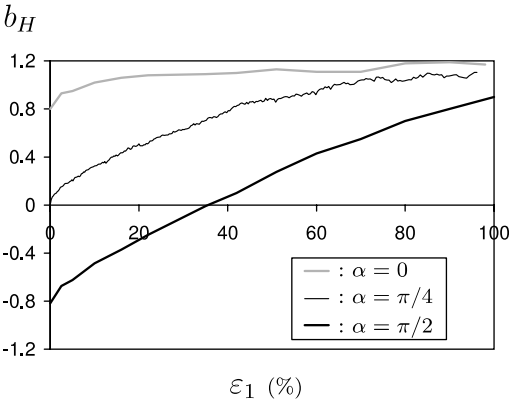

Fig. 34. Evolution of parameter b_H for samples with $R_a = 3$.

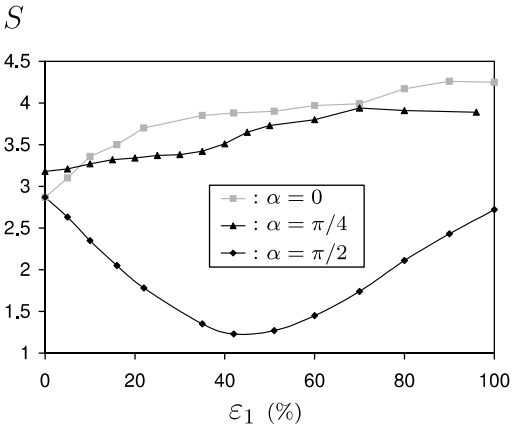

Fig. 35. Evolution of parameter S for samples with $R_a = 3$.

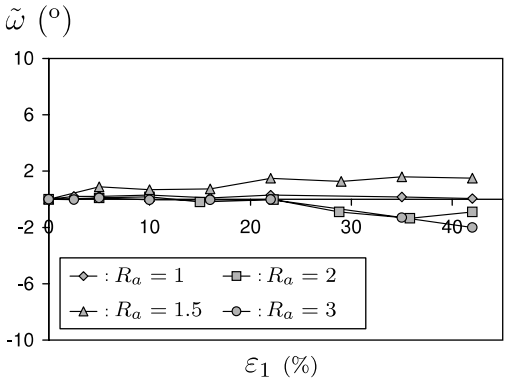

Fig. 36. Mean rotation of particles for $\alpha = 0$.

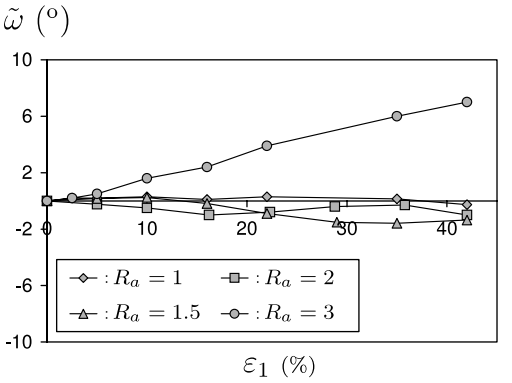

Fig. 37. Mean rotation of particles for $\alpha = \pi/2$.

The analysis of the internal variables b_H, b_A, S provides a more complete understanding of some results shown in Section 4. For example if we analyze Fig. 8(a), the samples seem to have reached the critical state for a major principal strain approximately equal to 35% which is not the case if the graph of void ratio is analyzed (Fig. 8(b)). At this stage, the internal states of samples ($\alpha = 0$, $\alpha = \pi/2$) are quite different in terms of void ratio and anisotropy. A same value of mobilized frictional angle actually results in a smaller void ratio (Fig. 8(b)) and smaller level of anisotropy in contact orientation (Fig. 16) for the sample loaded in direction $\alpha = \pi/2$. Though the residual mobilized angle of friction has been reached, the internal state of the sample does not correspond to the critical state yet. Even for a given loading condition ($\alpha = \pi/2$), a constant mobilized angle of friction that is obtained when ε_1 reaches 35% does not reflect a steady state of anisotropy since the internal structural is still evolving.

For the former sample, the process of reorientation for both contact orientation and particle orientation is completed whereas for the latter the particle orientation is almost isotropic. Then, the critical state is completely related to internal processes and the so called residual mobilized angle does not accurately reflect internal phenomena.

5.4. Rotation of particles $\tilde{\omega}$

For all particles except those with an aspect ratio equal to 3, the mean value of the local rotations is approximately equal to zero (Figs. 36 and 37) and the standard deviation is similar for all the particles (this standard deviation is far greater for particles with a circular shape, Nouguier-Lehon et al., 2003). For particles with an aspect ratio equal to 3 loaded in a direction which is perpendicular to the initial anisotropy, the mean value of the rotation is significantly different from zero and is linked to a continuous global rotation of all the particles in a given direction (Fig. 37). This result is not in agreement with the usual results, showing that the mean value of particle rotation is highly correlated with the rotation of the equivalent continuum (for biaxial tests this rotation is equal to zero). This might be because, for this kind of very elongated particle, a random rotation of particles would generate considerable dilatancy, so a bifurcation occurs in the behavior of the material.

6. Conclusions

Different points can be emphasized.

6.1. Critical state

The critical state (mobilized angle of friction, void ratio, anisotropy) can always be reached in granular material irrespective of particle shape and inherent anisotropy. Nevertheless for loadings which are applied in a different direction from the major principal direction of the contact anisotropy, the strain required to reach this state increases with the aspect ratio of particles. For example, for particle with an aspect ratio equal to 2, the critical state is reached for a major principal strain equal to 60% and for particle with an aspect ratio equal to 3, the critical state is to be reached for a major principal strain greater than 100%. Finally, a almost linear relationship was found between the macroscopical properties at the critical state (internal friction angle, void ratio) and the aspect ratio of particles.

6.2. Measurement of internal state

The coordination number N_c is not well correlated with the density variable only, since it does not take into account a very important parameter which is the shape of particles. Moreover, even for a considered material, this relation seems to depend on the stress path (particularly true for R_a greater than 2). Three measures of the internal texture anisotropy have been proposed and analyzed (b_H, b_A, S). They derive from the orientations of contact between grains ($\boldsymbol{H}$) and from the orientation of particles ($\boldsymbol{A}$). For particles with a low elongation ratio, parameters b_A and S may not be enough sensitive and in this case, $\boldsymbol{H}$ seems to be a more relevant measure of the internal state. For particles with more anisotropic shapes, b_H, b_A, S are highly correlated and consequently, measuring tensor $\boldsymbol{H}$ could be considered enough to characterize the internal anisotropy of granular materials. Nevertheless, parameter S that was defined allows a better understanding of phenomena for particles with high elongation ratios, since the deduced rate of anisotropy can always be compared with the maximum possible rate of anisotropy S_{max} for a sample with a given particle shape and the minimum anisotropy (actually the isotropic state) obtained for $S = 1$.

6.3. Influence of particle shape on the internal state; implications for the constitutive modelling of granular soils

The evolution of the internal state for granular materials composed of isotropic particles is essentially linked to the increase of contact number in the major principal direction of loading and the decrease of contact number in the orthogonal direction. For materials characterized by particles with a higher aspect ratio, two local phenomena take place: the contact orientation evolves and, if necessary (test condition: $\alpha = \pi/2$), the particles rotate so the preferential orientation of particles becomes perpendicular to the loading direction. These two phenomena are found to be highly correlated.

It can be emphasized that the initial anisotropy increases with the aspect ratio of particles (a consequence of the way samples are created). Moreover, this anisotropy hardly evolves as the aspect ratio of particles increases.

In the first approximation, initial anisotropy seems to plays a major role in the behavior of samples with highly anisotropic particles, whereas for samples with quasi isotropic particles this predominant role is assumed by the induced anisotropy.

A particular point is to be noted: when particles with an aspect ratio equal to 3 are loaded in a direction which does not correspond to the direction of initial anisotropy, the mean value of the local rotation of particles is significantly different from zero.

References

Biarez, J., Wiendieck, K., 1963. La comparaison qualitative entre l'anisotropie mécanique et l'anisotropie des milieux pulvérulents. Compte Rendu de l'Académie des Sciences 256, 1217–1220.

Calvetti, F., Combe, G., Lanier, J., 1997. Experimental micromechanical analysis of a 2D granular material: relation between structure evolution and loading path. Mechanics of Cohesive-Frictional Materials 2, 121–163.

Cambou, B., Dubujet, Ph., Nouguier-Lehon, C., 2004. Anisotropy in granular materials at different scales. Mechanics of Materials 36 (12), 1185–1194.

Chang, C.S., Misra, A., 1990. Packing structure and mechanical properties of granulates. Journal of Engineering Mechanics 116 (5), 1077–1093.

Cundall, P.A., Strack, O.D.L., 1979. A discrete numerical model for granular assemblies. Géotechnique 29 (1), 47–75.

Dedecker, F., Chaze, M., Dubujet, Ph., Cambou, B., 2000. Specific features of strain in granular materials. Mechanics of Cohesive-Frictional Materials 5 (3), 173–193.

Field, W.G., 1963. Towards a statistical definition of granular mass. In: Fourth Australian and New Zealand Conference on Soil Mechanics, pp. 143–148.

Jean, M., 1995. Frictional contact in collections of rigid or deformable bodies: numerical simulation of geomaterials. In: Salvadurai, A.P.S., Boulon, M.J. (Eds.), Mechanics of Geomaterials Interfaces. Elsevier, Amsterdam, pp. 463–486.

Jean, M., 1999. The non-smooth contact dynamics method. Computer Methods in Applied Mechanics and Engineering 177, 235–257.

Mirghasemi, A.A., Rothenburg, L., Matyas, E.L., 2002. Influence of particle shape on engineering properties of assemblies of two-dimensional polygon-shaped particles. Géotechnique 52 (3), 209–217.

Moreau, J.J., 1994. Some numerical methods in multibody dynamics: application to granular materials. European Journal of Mechanics, A/Solids 13 (4-suppl.), 93–114.

Moreau, J.J., 1999. Some basics of unilateral dynamics. In: Pfeiffer, F., Glocker, C. (Eds.), Unilateral Multibody Contacts. Kluwer, Dordrecht, pp. 1–14.

Nouguier-Lehon, C., Cambou, B., Vincens, E., 2003. Influence of particle shape and angularity on the behaviour of granular materials: a numerical analysis. International Journal for Numerical and Analytical Methods in Geomechanics 27 (14), 1207–1226.

Oda, M., Kazama, H., 1998. Microstructure of shear bands and its relation to the mechanisms of dilatancy and failure of dense granular soils. Géotechnique 48 (4), 465–481.

Poulos, S.J., 1981. The steady state of deformation. Journal of the Geoenvironmental Engineering Division, ASCE 105 (2), 201–255.

Radjaï, F., Troadec, H., Roux, S., 2004. Key features of granular plasticity. In: Antony, S.J., Hoyle, W., Ding, Y. (Eds.), Granular Materials: Fundamentals and Applications. Royal Society of Chemistry, pp. 157–183.

Roscoe, K.H., Schofield, A.N., Wroth, C.P., 1958. On the yielding of soils. Géotechnique 8 (1), 22–53.

Rothenburg, L., Bathurst, R.J., 1989. Analytical study of induced anisotropy in idealized granular materials. Géotechnique 39 (4), 601–614.

Rothenburg, L., Bathurst, R.J., 1992. Micromechanical features of granular assemblies with planar elliptical particles. Géotechnique 42 (1), 79–95.

Rothenburg, L., Kruyt, N.P., 2004. Critical state and evolution of coordination number in simulated granular materials. International Journal of Solids and Structures 41, 5763–5774.

Satake, M., 1978. Constitution of mechanics of granular materials through the graph theory. In: Cowin, S.C., Satake, M. (Eds.), US–Japan Seminar on Continuum-Mechanics and Statistical Approaches in the Mechanics of Granular Materials, pp. 47–62.

Thornton, C., Barnes, D.J., 1986. Computer simulated deformation of compact granular assemblies. Acta Mechanica 64, 45–61.